Characterization of biological features of a rat F98 GBM model: a PET-MRI study with [18F]FAZA and [18F]FDG

Nuclear Medicine and Biology 40 (6) 2013 ; 831-840

DOI: 10.1016/j.nucmedbio.2013.05.004

Characterization of biological features of a rat F98 GBM model: a PET-MRI study with [18F]FAZA and [18F]FDG

Sara Belloli[a,b,c], Andrea Brioschi[d], Letterio S. Politi[e], Francesca Ronchetti[d], Sara Calderoni[d], Isabella Raccagni[b], Antonella Pagani[e], Cristina Monterisi[a,b,c], Francesco Zenga[f,g], Gianpaolo Zara[h], Ferruccio Fazio[a,b,c], Alessandro Mauro[d,f], Rosa Maria Moresco[a,b,c,*]

[a]IBFM-CNR, Segrate, Italy
[b]Fondazione Tecnomed and Department of Health Sciences, University of Milan-Bicocca, Milan, Italy
[c]Department of Nuclear Medicine, San Raffaele Scientific Institute, Milan, Italy
[d]Istituto Auxologico Italiano, Department of Neurology and Neurorehabilitation, San Giuseppe Hospital, Piancavallo (VB), Italy
[e]Neuroradiology Department and Neuroradiology Research Group, San Raffaele Scientific Institute, Milan, Italy
[f]Department of Neuroscience, University of Turin, Turin, Italy
[g]City of Health and Science Hospital, Turin, Italy
[h]Department of Science and Technology of Drug, University of Turin, Turin, Italy

*Corresponding author. Università degli Studi di Milano-Bicocca, Via Fratelli Cervi, 93, 20090 Segrate, Milan, Italy. Tel.: +39 02 2643 3817; fax: +39 02 2641 5202. E-mail address: moresco.rosamaria@hsr.it (R. M. Moresco).

Abstract

Introduction. The prognosis of malignant gliomas remains largely unsatisfactory for the intrinsic characteristics of the pathology and for the delayed diagnosis. Multimodal imaging based on PET and MRI may assess the dynamics of disease onset and progression allowing the validation of preclinical models of glioblastoma multiforme (GBM). The aim of this study was the characterization of a syngeneic rat model of GBM using combined in vivo imaging and immunohistochemistry.
Methods. Four groups of Fischer rats were implanted in a subcortical region with increasing concentration of rat glioma F98 cells and weekly monitored with Gd-MR, [^{18}F]FDG- and [^{18}F]FAZA-PET starting one week after surgery. Different targets were evaluated on post mortem brain specimens using immunohistochemistry: VEGF, GFAP, HIF-1α, Ki-67 and nestin.
Results. Imaging results indicated that tumor onset but not progression was related to the number of F98 cells. Hypoxic regions identified with [^{18}F]FAZA and high-glucose metabolism regions recognized with [^{18}F]FDG were located respectively in the core and in external areas of the tumor, with partial overlap and remodeling during disease progression. Histological and immunohistochemical analysis confirmed PET/MRI results and revealed that our model resumes biological characteristics of human GBM. IHC and PET studies showed that necrotic regions, defined on the basis of [^{18}F]FDG uptake reduction, may include hypoxic clusters of vital tumor tissue identified with [^{18}F]FAZA. This last information is particularly relevant for the identification of the target volume during image-guided radiotherapy.
Conclusions. In conclusion, the combined use of PET and MRI allows in vivo monitoring of the biological modification of F98 lesions during tumor progression.

***Keywords*:** GBM model; Glucose metabolism; Hypoxia; Immunohistochemistry; MRI; PET.

1. Introduction

Gliomas are the most common primary Central Nervous System (CNS) neoplasms, accounting for 30% of all primary CNS tumors and 80% of malignant ones in adult. Glioblastoma multiforme (GBM) represents the most malignant form, still maintaining poor prognosis in spite of the use of more aggressive therapeutic schedule (such as surgery plus radiation therapy and chemotherapy) and the adoption of increasingly suitable supportive care (median survival rate equal to 14.6 months and estimated five-year relative survival value in United States equal to 4.7%) [1]. The prognosis of these tumors remains largely negative, due to both specific characteristics of gliomas, such as lack of clear clinical signs in the early stages of disease, early infiltrative tendency and extreme genotypic and phenotypic heterogeneity, and the presence of the blood–brain barrier (BBB), which makes difficult the attack of drug therapies effective in other locations [2] and [3]. Magnetic resonance imaging (MRI) is the modality of choice for the evaluation of a patient with suspected or confirmed glioblastoma multiforme. However, even with the precise morphological information obtained by T2w and post-contrast T1 sequences, conventional MRI alone cannot reveal the complex and heterogeneous biological features of this tumor. Histo-pathological hallmarks of GBM include high cell proliferation, anaerobic glycolysis, presence of a necrotic core and active angiogenesis, leading to vessels with morphological abnormalities. Vascular abnormalities contribute to the presence of hypoxic regions that, according to recent data, might sustain invasion, apoptosis, stem cells recruitments and resistance to treatment including radiation therapy.

PET allows the in vivo imaging of different functional and molecular properties of tumors including the presence of regions with reduced oxygen concentration. Using PET and [^{18}F]Fluoromisonidazolo ([^{18}F]MISO) as radioligand, it has been shown that in patients with GBM, hypoxia strongly correlated with poor time to progression and survival [4]. Another imidazole derivative, [^{18}F]Fluoroazomycin arabinoside ([^{18}F]FAZA), characterized by higher signal to noise ratio in comparison with [^{18}F]MISO [5], has been recently and successfully used for the in vivo imaging of hypoxic regions in GBM patients [6].

As previously stated, tissue hypoxia, through the activation of the transcription factor HIF-1α (Hypoxia Inducible Factor) modulates the expression of several genes [7] and [8] including those controlling the glycolytic pathway like glucose transporter (GLUT) and hexokinase (HK). Recent findings indicate that GLUT-1 and HK2 levels are related to tumor aggressiveness and patients' overall survival [9] and [10]. The anaerobic glycolysis, known as Warburg effect, can be visualized by PET using the glucose analogue 2[F-18]fluoro-2-deoxy-D-glucose ([^{18}F]FDG). In brain tumor, the increase in glucose metabolism is predictive of patient survival [11] and 12] and response to radiation therapy [13]. The poor outcomes for patients with GBM require improved therapies and complementary diagnostic imaging to monitor and optimize treatment strategies. A number of targeted therapies acting on EGFR, VEGF, PI3K/AKT/mTOR pathways, administered alone or in combination, are under evaluation [14] and [15]. However, most of these drugs act on pathways that are heterogeneously expressed in tumors and methods for the early assessment of treatment efficacy are needed. Since a variety of therapies under development modulate tumor metabolism and hypoxia, radiopharmaceuticals like [^{18}F]FDG and [^{18}F]FAZA may represent potential imaging biomarkers for the early identification of responder patients. In addition, [^{18}F]FAZA-PET may be useful in identifying hypoxic radiation resistant regions that may require boost doses during radiotherapy. In order to test the potential use of PET imaging for the evaluation of treatment response, the use of animal models that reproduce human GBM is particularly relevant. Among the various models existing, the syngeneic Fischer/F98 rat seems to resemble the histopathological and clinical features of human GBM. F98 cells, deriving from an N-ethyl-N-nitrosourea induced anaplastic glioma, show low immunogenicity when implanted in syngeneic host and produce infiltrative tumor resistant to conventional treatment. In addition, as human GBM, this model over-expresses targets like *PDGFβ*, *Ras*, *EGFR*, *cyclin D1* and *cyclin D2* [16]. Considering imaging studies, MRI shows enhanced

gadolinium contrast regions at T1-weighted images corresponding to areas of blood brain barrier disruption or incomplete formation in neoangiogenic vessels, and significant peritumoral edema at T2-weighted images, while PET shows a net increase in [^{18}F]FDG uptake [17]. In this study, we further evaluated this animal model to identify similarities with human GBM using in vivo imaging to monitor tumor growth and morphology (Gd-MR), metabolism ([^{18}F]FDG-PET) and regional hypoxia ([^{18}F]FAZA-PET). Despite the availability of other ligands more useful for the clinical management of patients with brain tumor, we decided to use [^{18}F]FDG and [^{18}F]FAZA for the characterization of F98 model since both trace two typical hallmarks of human GBM strictly related with each other like increased glucose metabolism and hypoxia. In addition, in vivo imaging results were compared with cell proliferation (ki-67), differentiation (Nestin), angiogenesis (VEGF) and hypoxia (HIF-1α) measured post mortem by immunohistochemistry techniques.

2. Materials and methods

2.1. Cell cultures

Rat F98 glioma cells were obtained from ATCC (Manassas, VA, USA) and maintained in a humidified incubator gassed with 5% carbon dioxide (37 °C) with DMEM (Dulbecco's Modified Eagle's Medium) supplemented with 10% FBS (Fetal Bovine Serum), 1% sodium pyruvate, 1% penicillin/streptomycin, 4 mM L-glutamine and 1.5 g/L $NaHCO_3$. The day of the surgery, cells were trypsinized, centrifuged, counted (with trypan blue) and resuspended at different concentration ranging between 10^2 and 10^5 cells/2 μl of PBS (all reagents from Life Technologies, Carlsbad, CA).

2.2. Animals

Male Fischer rats (Charles River, Wilmington, MA) weighting 200 g (mean 210 ± 12.7 g) were housed in standard facilities, handled and maintained according to our Institutional Animal Care and Use Committee ethical regulations.

2.3. Glioma rat model

For intracranial implantation of F98 cells, rats were anesthetized by intraperitoneal injection (i.p.) of tiletamine and zolazepan (25 mg/kg and 25 mg/kg both from Sigma-Aldrich, St. Louis, MO) and placed in a stereotactic frame. The head was shaved and the skin accurately cleaned before incision in the midline. The skull was drilled using a micro-burr and a 5 μl-Hamilton syringe was inserted in the hole for the injection of the cells in the right sub-thalamic region identified by the stereotactic coordinates: AP = 3; L = 2; V = 5. Different concentrations of F98 cells (10^2, 10^3, 10^4 and 10^5) suspended in 2 μl of PBS were used. After the injection, the needle was left in place for additional 5 min and then slowly withdrawn; holes were sealed with bone wax and the incision was sutured. Rats were reported in their cage and monitored until awakening from anaesthesia.

2.4. Study design

A total of 36 rats were treated, subdivided into 4 groups according to the amount of implanted cells (10 animals for 10^5, 12 for 10^4, 8 for 10^3 and 6 for 10^2 implanted cells) and daily monitored to detect neurological symptoms and signs (cognitive and motor impairments such as lethargy, hemiplegia, weight loss). One week after implantation, all animals started weekly recordings of Gd-MRI data, till the development of MRI-detectable tumors (early stage). From this point, rats were analyzed weekly also with PET-[^{18}F]FDG and -[^{18}F]FAZA (this last only for 10^5 and 10^4 groups) until death or sacrifice because of severe neurological and motor impairment signs (late stage).
Two additional animals for each group were sacrificed by transcardiac perfusion at both early and late stage of tumor progression and brains dissected for histological and immunohistochemical analyses.

2.5. In vivo monitoring

Immediately before the MRI study, animals were anesthetized (i.p.) with tribromoethanol 1.7% solution (20 μl/g of rat weight) and 0.3 mmol/kg of gadobutrolo (Gadovist®, Bayer) was injected in the tail vein. MRI was performed using a 3 T human-grade MRI scanner (Achieva 3 T, Philips Medical Systems, The Netherlands) equipped with a rat dedicated volumetric coil of 40 mm diameter (Rat Coil, Philips Medical Systems, The Netherlands). Rats were positioned prone on temperature controlled MRI bed and a Spin Echo T1 weighted sequence (TR 600 ms, TE 16 ms, field of view 40 mm, acquired voxel dimension 0.16 × 0.2 × 0.75 mm, 54 slices) was acquired on the coronal plane. The tumor volume and the absolute necrotic volume were calculated by an expert neuroradiologist on a separate workstation (Easy Vision, Philips Medical Systems, The Netherlands) upon manual segmentation of the lesion on the basis of signal intensity variation and enhancement characteristics using a dedicated software. Once reconstructed, images were exported in Analyze format for PET-MRI co-registration using PMOD 2.7 software.

[^{18}F]FDG is prepared in our facility for clinical use (European Pharmacopoeia VII ed.), while [^{18}F]FAZA was obtained using the radiosynthesis procedure previously described by Reischl with minor modifications [18]. Both radiotracers were injected with a radiochemical purity higher than 99%.

The day of PET study, animals were injected in a tail vein with 35.51 ± 2.23 MBq for [^{18}F]FDG or 27.11 ± 2.69 MBq for [^{18}F]FAZA. Before acquisition, rats were pre-anesthetized using ether and positioned prone on the tomograph bed with the head centred in the tomograph field of view (YAP-(S)-PET II, I.S.E. s.r.l., Italy). During acquisition, animals were kept under gas anaesthesia (2% Isoflurane in air). [^{18}F]FDG-PET scans started 60 min after injection and lasted 30 min, while [^{18}F]FAZA-PET acquisitions started after 120 min and lasted 15 min [5]. PET data were acquired in list mode using the full axial acceptance angle of the scanner (3D mode) and then reconstructed with expectation maximization (EM) algorithm [19].

2.6. Image quantification

2.6.1. VOI analysis

PET images were calibrated with a dedicated phantom, corrected for isotope half-life and co-registered with MR images using PMOD 2.7 software using a manual procedure. The radiotracers uptake of tumoral and background regions was calculated using a volume of interest (VOI) analysis on PET-MRI co-registered images. Tumor was automatically defined on transaxial slices using the tool "automatic isocontour detection" and thresholding signal half way between mean background and maximum pixel value [20]. Background region was defined drawing on three consecutive transaxial slices elliptical regions of interest (VOI volume = 17.0 ± 3.2 mm^3) in a cerebral non-cancerous area adjacent to tumor. Radioactivity concentration was expressed as Standardized Uptake Value (SUV) according to the formula:

$$SUV = (Region\ radioactivity/Injected\ radioactivity) * animal\ weight.$$

Tumor uptake data were also calculated as tumor-to-background ratio (T/B) dividing the maximum SUV obtained for tumor by the mean SUV found in background region.

2.6.2. Segmentation analysis

Segmentation analysis was performed using PMOD 2.7 software on PET-MRI co-registered images of animals evaluated with both [^{18}F]FAZA and [^{18}F]FDG. After VOI's definition, tumor image was automatically extracted using "mask voxels outside VOI" tool and resulting region used to isolate hyper-metabolic or hypoxic areas and to visualize the overlap of the two signals in the same animal in all the studies performed.

2.7. Ex-vivo analysis

Under anaesthesia with tiletamine and zolazepan (25 mg/kg and 25 mg/kg), rats were sacrificed by transcardiac perfusion of 4% phosphate-buffered paraformaldehyde (pH 7.4–7.5; Sigma-Aldrich). Brains were collected, dehydrated and paraffin embedded. Slices of 5 microns were cut, mounted on poly-L-lysine coated slides and processed to highlight tumor characteristics. H&E (Haematoxylin and Eosin, Sigma-Aldrich) were used to evaluate cell morphology, mitotic figures, infiltrative modality of glioma and necrotic areas. Immunohistochemistry labelling was assessed for GFAP (Glial Fibrillary Acid Protein), Nestin, VEGF (Vascular Endothelial Growth Factor), Ki-67 and HIF-1α markers.

2.7.1. H&E staining

Slides were deparaffinised, rehydrated and then dip for 30 s in haematoxylin (Mayer's hemalum solution; Merck Millipore, Billerica, MA), rinsed in tap water and briefly immersed in 1% eosin (Eosin Y yellowish; Merck Millipore); after wash in water, slides were finally dehydrated and mounted in DPX (Sigma-Aldrich).

2.7.2. Immunohistochemistry

Immunohistochemistry was performed with the Vectastain elite ABC kit (Vector Laboratories, Burlingame, CA), following manufacturer's instructions. Slides were deparaffinised and rehydrated; subsequently, microwave antigen unmasking was performed for either cytoplasmic (1 mM EDTA, pH 8.0) or nuclear (10 mM citrate buffer-Tween 20, pH 6) epitopes (1 min 750 W + 1 min 100 W). Samples then underwent 3% H_2O_2 endogenous peroxidase quenching (30 min) and blocking with either goat (Dako, Glostrup, Denmark) or horse (Vector Laboratories) normal serum for 1 h. Incubation with primary antibodies was carried out overnight at 4 °C: anti-GFAP (1:2000, Rabbit Polyclonal, DAKO), anti-HIF-1α (1:500, mouse monoclonal, Novus Biological, Littleton, CO), anti-Ki67 (1:1000, Rabbit Polyclonal, Merk Millipore), anti-Nestin (1:1000, Mouse Monoclonal, Merk Millipore), anti-VEGF (C-1) (1:200, Mouse Monoclonal, Santa Cruz Biotechnology, Santa Cruz, CA). Incubation with secondary anti-rabbit (1:100, Dako) or anti-mouse (1:100, Vector Laboratories) biotinylated IgG was performed for 30 min at RT and then samples incubated 1 h with avidin biotin complex. Peroxidase reaction was visualized with 0.15 mg/ml DAB (3,3′-diamino-benzidine, Sigma-Aldrich, Milan, IT) plus 0.025% hydrogen peroxide in 0.05 M Tris–HCl buffer pH 7.6. Slides were finally counterstained with haematoxylin, dehydrated and mounted with DPX.

Sample pictures were acquired trough a system composed of a Leica microscope equipped with Leica DFC320 video camera and connected to a PC.

In order to estimate the growth rate of tumors, the percentage of tumor cells expressing the proliferation marker Ki-67 was measured. A proliferation index was calculated for each tumor by counting the total number of tumor cell nuclear profiles and the number of Ki-67-positive nuclear profiles in three randomly selected fields per slice (three slices per rat brain).

Fields images (40 ×) were acquired and then counting performed with the Neurolucida 7 software (MBF Biosciences, Williston, VT), using the "Particles and Tracing" application.

2.7.3. Immunofluorescence

Double-immunofluorescence was performed to detect possible co-localization of GFAP and nestin markers. Sections were incubated overnight with anti-GFAP and anti-nestin (same antibodies specified above) and 1 h RT with Alexa Fluor 555-conjugated anti-rabbit IgG and Alexa Fluor 488-conjugated anti-mouse IgG antibodies (5:1000, Life Technologies). All pictures were collected using the Bio-Rad confocal microscope Radiance 2100 (with Argon/HeNe lasers) coupled to an inverted Nikon Eclipse TE2000 microscope (method: Ex488/Ex543, 560DCLP filter, HQ515/30 for green and 600LP emission filter for red).

3. Results

3.1. In vivo monitoring: tumor onset and survival curve

Table 1 summarizes disease onset with corresponding tumor volume and animal survival of the four different groups of rats based on Gd-MR imaging. In rats implanted with 10^2 cells, tumors appeared at the third week of monitoring with a longer survival (24 days) and a mean tumoral volume at onset of 0.04 ± 0.01 cm^3. Due to the severe neurological and physical conditions consisting of motor impairment (hemiparesis, ataxia), intracranial pressure with eye bleeding and loss of 8.8% ± 3.6 of initial mass weight, animals were sacrificed before any further imaging examination. In rats implanted with 10^3 cells, tumors appeared one week before the group implanted with 10^2 cells (14 days from surgery) with a mean volume measured by Gd-MR of 0.08 ± 0.05 cm^3. Animals began to show signs of severe illness starting from the third week and were then sacrificed. In animals injected with 10^5 and 10^4 cells, lesions appeared 7 days after cell implantation. In both groups, MRI mean tumor volume was 0.11 ± 0.1 cm^3. One rat per group was able to perform an additional imaging section in the next week, the rest died or were sacrificed.

Table 1. Schematic representation of tumor onset and the corresponding volume of Gd-MR enhancement, [^{18}F]FDG- and [^{18}F]FAZA-PET signals on the basis of implanted cells concentration.

Tumor onset			Mean tumor volume (cm^3 ± SD)		
F98 cells concentration	Tumor onset Gd-MR (days)	Mean survival (days ± SD)	Gd-MR	[^{18}F]FGD-PET	[^{18}F]FAZA-PET
10^2	21	24.0 ± 0.0	0.04 ± 0.01	0.04 ± 0.02	–
10^3	14	17.0 ± 0.0	0.08 ± 0.05	0.05 ± 0.04	–
10^4	7	11.8 ± 2.1	0.12 ± 0.03	0.08 ± 0.03	0.04 ± 0.02
10^5	7	14.0 ± 1.7	0.11 ± 0.11	0.06 ± 0.03	0.04 ± 0.01

Summarizing, the time of tumor onset progressively decreased with increasing concentration of F98 cells injected (Fig. 1). By contrast, when tumor appeared, the time course of the disease was comparable in the different groups of animals analyzed regarding duration (5.9 ± 2.2 days), aggressiveness and invasiveness.

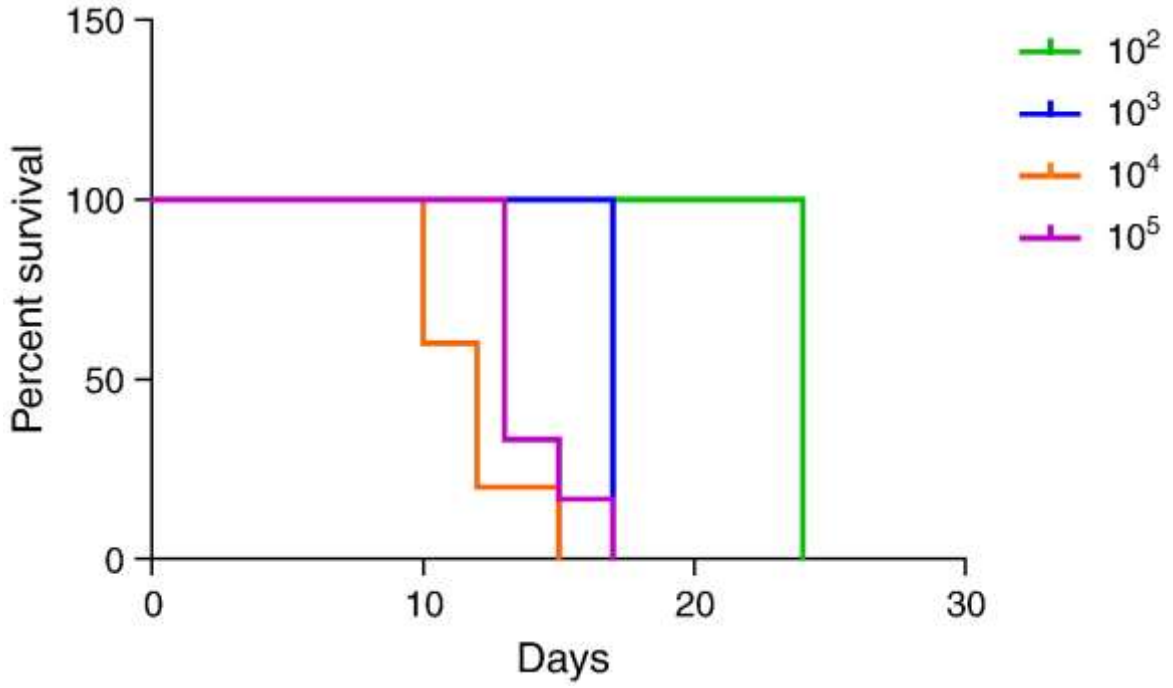

Fig. 1. Survival curve of rats implanted in the right sub-thalamic brain region with several F98 cells concentrations.

3.2. Image quantification

MRI studies showed areas of contrast enhancement around cell implantation site at 21 days in animals with 10^2 cells (Fig. 2A) and at 14 days in animals with 10^3 cells (Fig. 2B). In this second group, the tumor volumes measured by MRI were larger than those measured by PET, on the contrary PET and MRI tumor volumes resulted comparable in animals implanted with 10^2 cells (Table 1). In both groups, high [^{18}F]FDG uptake was localized inside MRI contrast enhancing regions, with a mean Standardized Uptake Value (SUV_{max}) of 3.33 ± 0.64 and a mean tumor to background ratio (T/B) value of 1.83 ± 0.08. In animals injected with 10^4 and 10^5 cells, gadolinium enhancing regions were detectable at MRI seven days after cells implantation (Fig. 2C and D). Like for the other groups of rats, lesions were hypermetabolic and [^{18}F]FDG uptake, expressed as SUV_{max}, was 3.59 ± 0.65, resulting in a T/B value of 1.5 ± 0.30. PET studies performed with [^{18}F]FAZA showed in animals injected with 10^4 and 10^5 F98 cells the presence of hypoxic regions localized in the core of the lesion visualized by MRI. Mean [^{18}F]FAZA SUV_{max} was for both groups 0.33 ± 0.06, with a mean T/B value of 2.19 ± 0.37. Hypoxic areas were less extended than hypermetabolic and gadolinium enhancing regions. In fact, mean tumor volumes were: 0.11 ± 0.6 cm^3 for MRI, 0.07 ± 0.04 cm^3 for [^{18}F]FDG and 0.03 ± 0.01 cm^3 in case of [^{18}F]FAZA. Regions of [^{18}F]FDG uptake were always greater than those of [^{18}F]FAZA and only partially overlapped. [^{18}F]FDG uptake areas were localized in the peripheral regions of MRI positive volume, whereas [^{18}F]FAZA was taken up mainly around the original injection site.

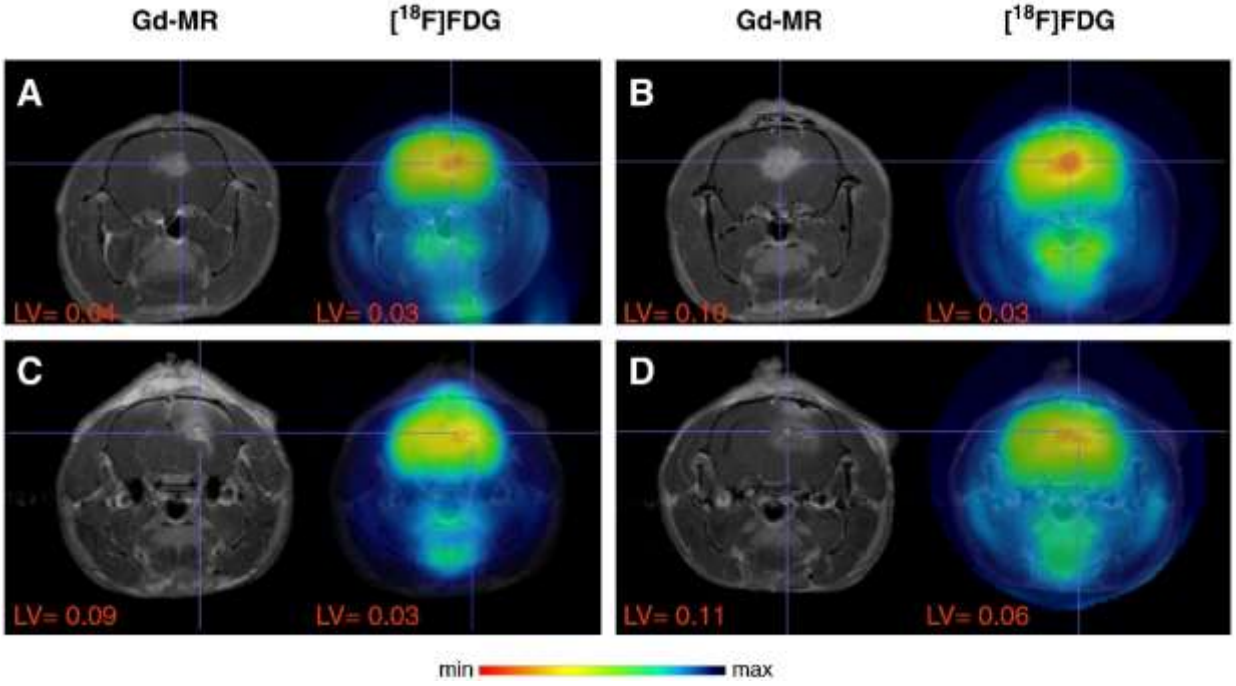

Fig. 2. Example of coronal Gd-MR (left) and Gd-MR-[^{18}F]FDG-PET co-registered images (right) of an animal implanted in a sub-thalamic region with 10^2 (A), 10^3 (B), 10^4 (C) and 10^5 (D) F98 cells at the first positive scan. For MRI acquisition, animals were anesthetized with 1.7% Tribromethanol, injected in a tail vein with 0.3 mmol/kg of gadobutrolo and after checking the correct centring of the brain, a T1-weighted Spin Echo sequence of a total of 20 min was acquired. For PET acquisition, animals were injected in a tail vein with 35.51 ± 2.23 MBq of [^{18}F]FDG, anesthetized with 2% Isoflurane and acquired for 30 min (6 scans of 5 min each). LV = lesion volume in cm^3.

Only two rats (one for 10^4 and one for 10^5 cells) survived more than two weeks performing a second set of MRI and PET studies (14 days post-surgery) (Fig. 3). Both animals showed increased lesion volumes at MRI (2.4-fold mean increase, from a mean volume of 0.11 ± 0.1 cm^3 to a mean volume of 0.42 ± 0.17 cm^3) which were much more hyperintense at periphery (edema). In addition, in the follow-up MRI study small necrotic areas of absence of contrast enhancement were observed. Further, the lesions presented ill-defined margins, resembling the imaging features of human GBM.

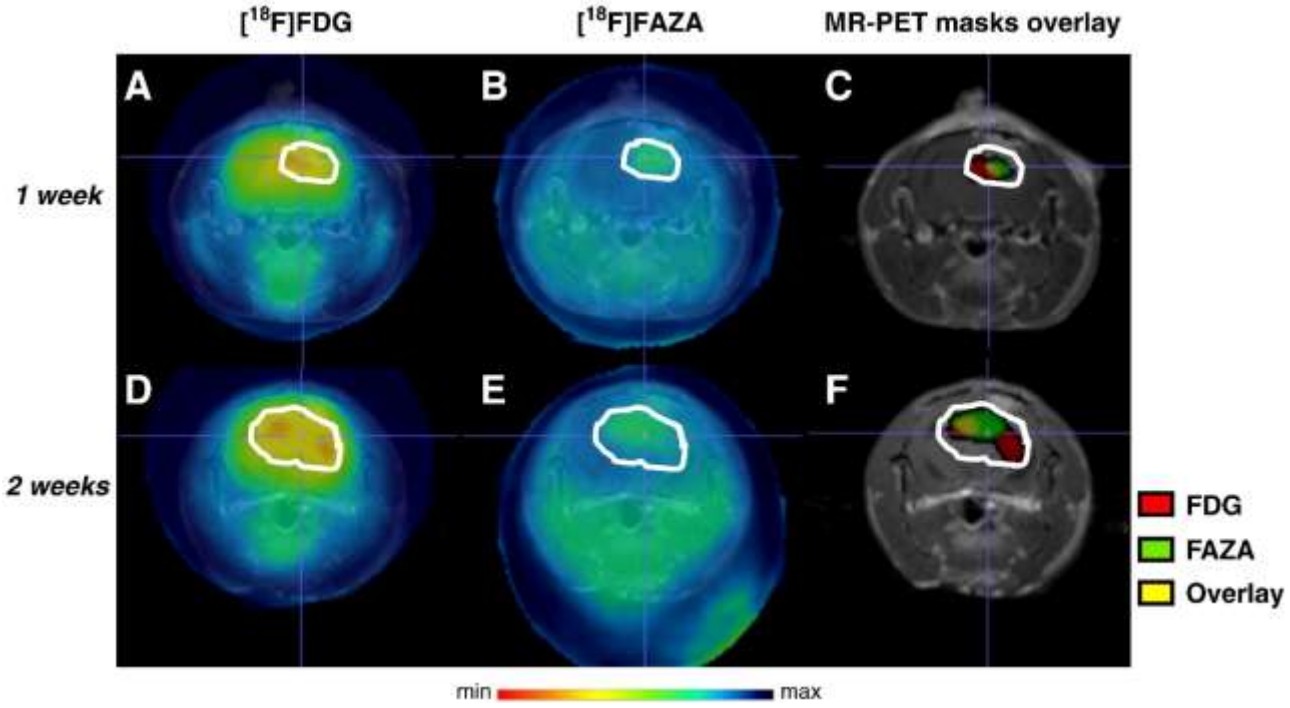

Fig. 3. Coronal Gd-MR and [^{18}F]FDG- and/or [^{18}F]FAZA-PET co-registered images of an animal implanted with 10^5 F98 cells. Top, imaging at the first Gd-MR positive scan with: (A) [^{18}F]FDG-PET, (B) [^{18}F]FAZA-PET, (C) [^{18}F]FDG/ [^{18}F]FAZA-PET fusion (segmentation analysis). Bottom, imaging of the same animal one week later: (D) [^{18}F]FDG-PET, (E) [^{18}F]FAZA-PET, (F) [^{18}F]FDG/[^{18}F]FAZA-PET fusion (segmentation analysis). For MRI acquisition, animals were anesthetized with 1.7% Tribromethanol, injected in a tail vein with 0.3 mmol/kg of Gadobutrolo and after checking the correct centring of the brain, a T1-weighted Spin Echo sequence of a total of 20 min was acquired. For PET acquisition, animals were injected in a tail vein with 35.51 ± 2.23 MBq of [^{18}F]FDG or 27.11 ± 2.69 MBq of [^{18}F]FAZA, anesthetized with 2% Isoflurane and acquired for 30 min or 15 min respectively. White lines: contour of tumoral area detected with Gd-MR.

[^{18}F]FDG positive areas increased of 2.5-fold over time (from a mean volume of 0.064 ± 0.03 cm^3 to a mean volume of 0.180 ± 0.13 cm^3) but with reduced level of radioactivity concentration (mean SUV_{max} value − 22%) particularly in the central region. On the contrary, [^{18}F]FAZA uptake consistently increased in terms of both volume (2.9-fold mean increase, from a mean volume of 0.038 ± 0.01 cm^3 to a mean volume of 0.086 ± 0.04 cm^3) and amount of radioactivity uptake (mean SUV_{max} value + 38%).

3.2.1. Segmentation analysis

The "Segmentation analysis" more clearly highlights the different pattern of distribution of the two radiotracers and the overlapping area in the animals analyzed over time (Fig. 3). In particular, [^{18}F]FDG was initially localized in the peripheral areas of the lesion (Fig. 3A), while [^{18}F]FAZA positive areas were limited into the core (Fig. 3B); overlapping area was very small and centred in the Gd-MR positive region (Fig. 3C). At the second evaluation, [^{18}F]FDG distribution followed the direction of tumor growth moving toward poles (Fig. 3D), while [^{18}F]FAZA increased its area of uptake remaining in the original area of sprouting (Fig. 3E). In this case, overlapping area enlarged and was positioned in the original part of the lesion (Fig. 3F).

3.3. Ex-vivo analysis

3.3.1. H&E

All the samples analyzed for each group of cell concentration showed the presence of large tumor with centrally located necrotic area, numerous mitotic figures meaning a high proliferative tumor rate and an evident perivascular invasion of neoplastic cells (Fig. 4).

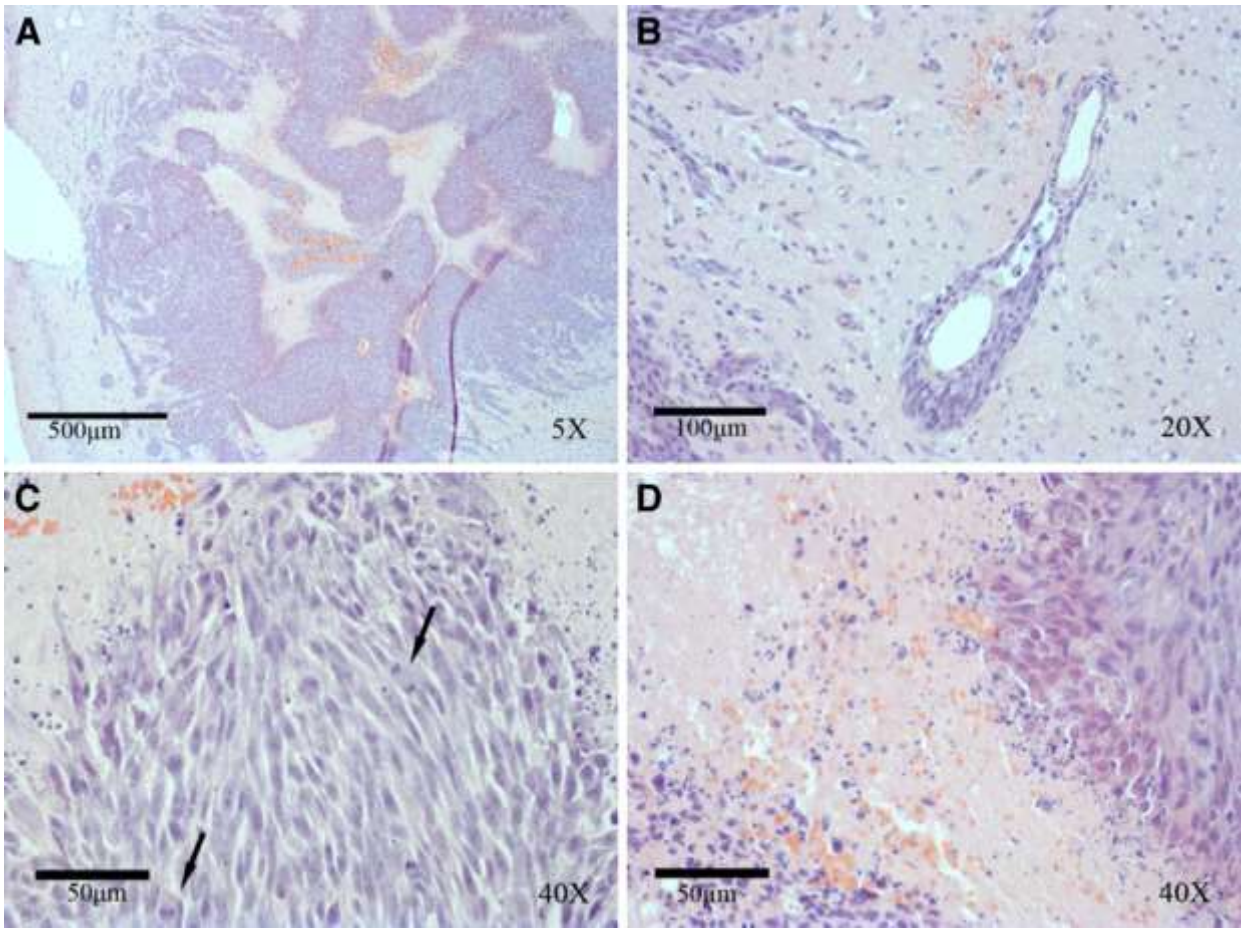

Fig. 4. H&E staining shows large tumors with central necrotic areas (A), oedema and perivascular invasion (B), mitotic cells (C) and necrosis (D).

Necrotic areas enlarged and changed distribution with tumor increasing size during time (Fig. 5A and B).

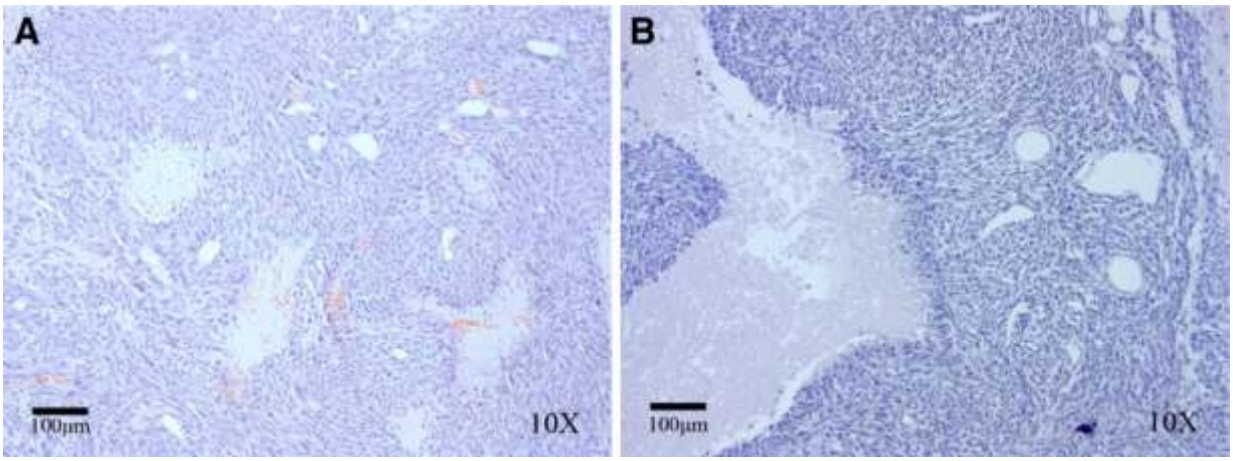

Fig. 5. H&E staining: example of tumoral necrosis evolution during disease progression (10^5 cells) at onset (A) or after later point of monitoring (B).

3.3.2. Immunohistochemistry and Immunofluorescence

Tumors from all implanted rats showed a GFAP staining that was strongly expressed from peripheral reactive glia (Fig. 6A) while few tumoral cells resulted positive (in 10^2 cells the staining was overall weaker than in other concentrations). Moreover, in all concentrations, there was a very strong nestin expression in tumoral cells (Fig. 6B) co-localized with GFAP positive reactive astrocytes (Fig. 6C-E) in peripheral margins within neoplasm and brain parenchyma.

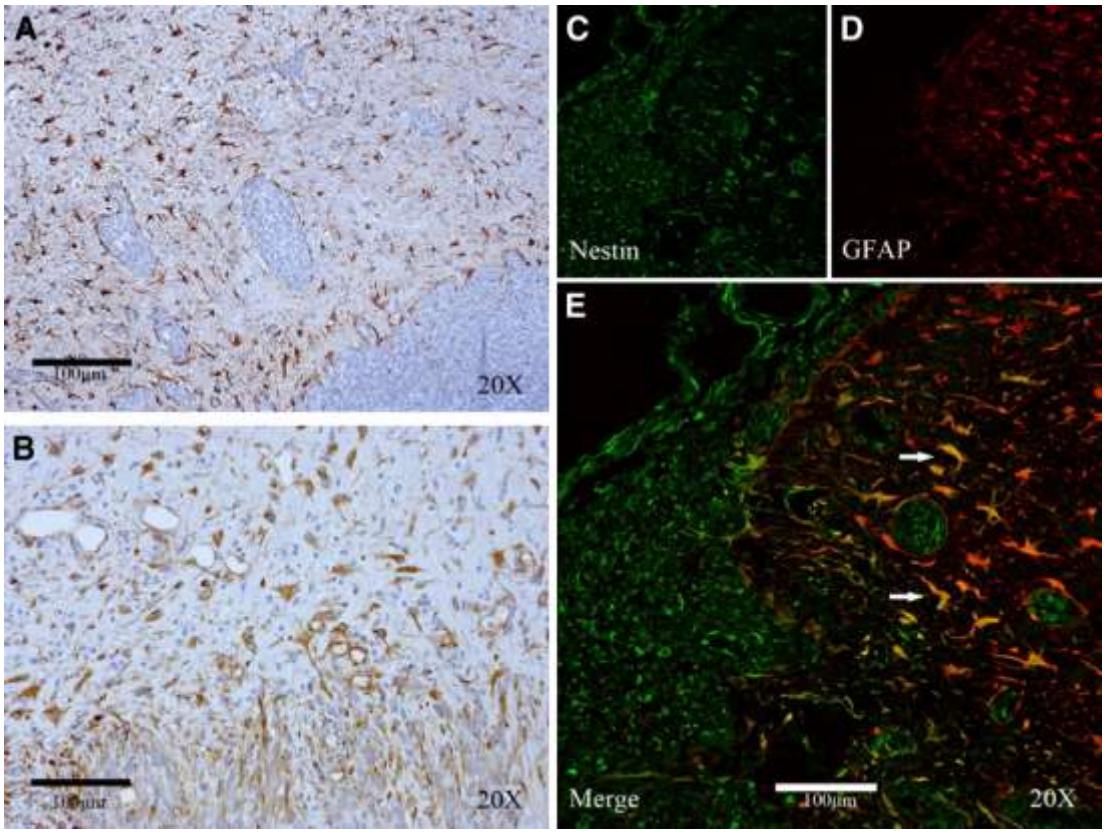

Fig. 6. Expression of GFAP (A) and nestin (B) in glioma of rat implanted with 10^5 cells. Confocal analysis of the two markers (C-D) and their merge (E).

All glioblastomas showed similar histopathological hallmarks, such as high VEGF positivity in tumoral cells and in neurons surrounding oedematous areas (Fig. 7A and B). HIF1-α staining was localized in hypoxic peritumoral cells (mainly neurons) and in few cells around necrotic areas (Fig. 7C and D); moreover, a great Ki-67 expression (Fig. 7E and F) was present, with an estimated proliferation index of 46%.

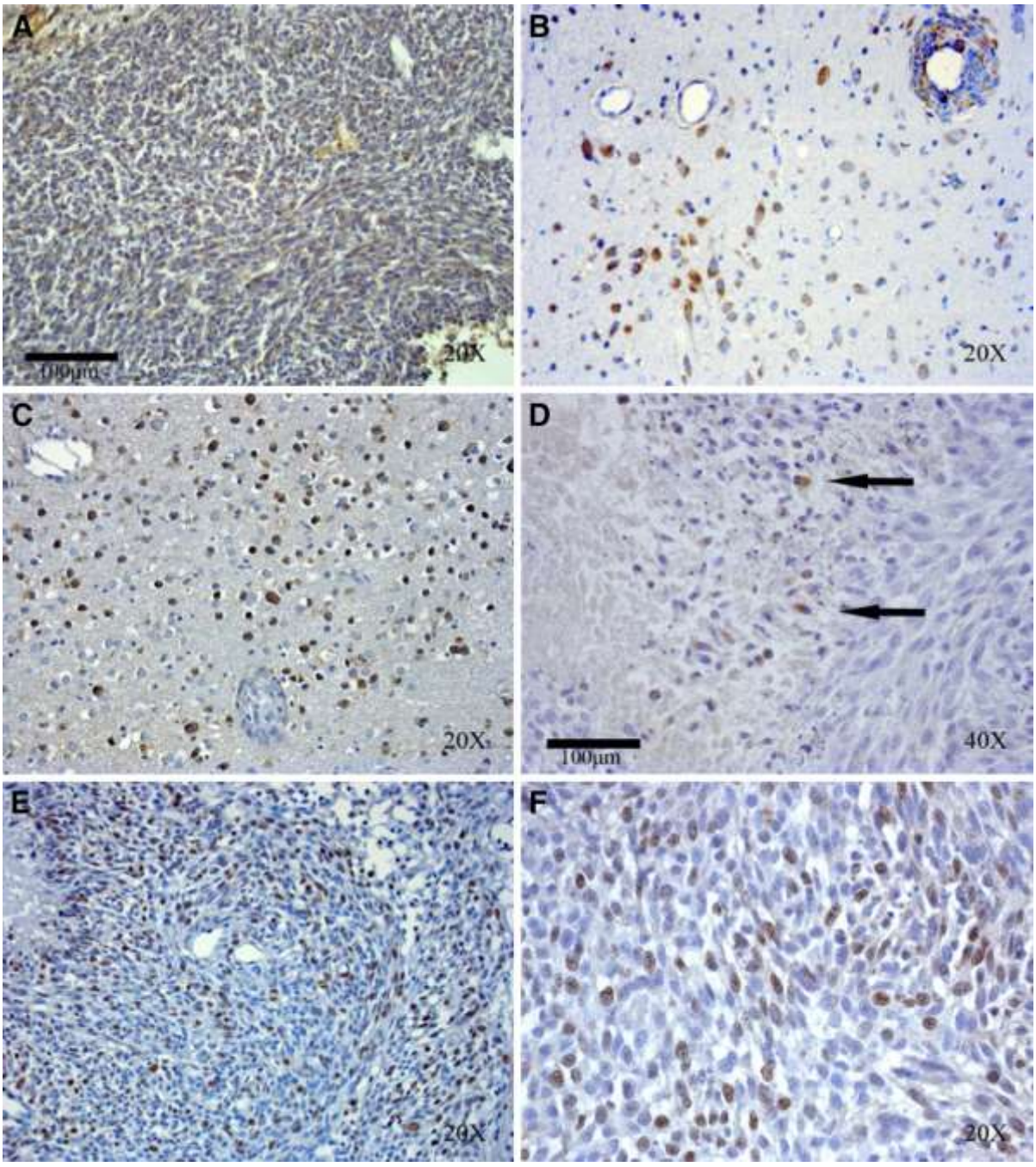

Fig. 7. Example of VEGF expression in the tumor mass (A) and in neurons surrounding oedematous areas (B); HIF1-α staining of ischemic neurons nearby the tumor (C) and in necrotic areas (D); Ki67 positivity of the glioma (E,F).

4. Discussion

Rat syngeneic F98 is a brain tumor model that reproduces the biological behaviour of human GBM and is therefore of particular interest for the preclinical evaluation of novel therapeutic approaches. The F98 model is based on the intracerebral implantation of high-grade glioma rat cells, which progressively induce the growth of weakly immunogenic tumor masses [21]. Like human GBM, it is highly proliferative and vascularised and infiltrates in brain parenchyma.

In this study, we further validated the F98 rat GBM model by combining in vitro histo-pathological with in vivo MRI and PET imaging results. As previously observed by other authors [17], surgical procedure was highly reproducible giving rise to tumor masses in the expected site of injection in 95% of implanted animals (34 of 36 injected rats). Concerning the clinical symptoms, animals developed cognitive and motor impairments (lethargy, hemiplegia, weight loss) which are typical of a high-grade glioma (IV grade) and which have already been described [17].

Since the relationship between amount of implanted cells and tumor development was not fully described, in this study we also evaluated the effect of increasing concentrations of F98 cells. We observed that once the lesions became visible at Gd-MR, survival time was 6 ± 2 days (range: 4 to 11), independently from the number of cells implanted. On the contrary, lesion onset, as well as the overall survival time of animals, was inversely related to the number of cells injected, thus confirming what was previously described by Mathieu and colleagues [17].

In clinical research and practice it is well known that the amount of [^{18}F]FDG uptake is positively related with tumor grade [11] and [22], whereas [^{18}F]FDG lesion volume is a negative prognostic factor in terms of illness progression and response to therapy [13]. As in the case of human GBM, in the F98 model we observed hypermetabolic lesions at [^{18}F]FDG-PET [23] and [24] giving a tumor-to-non tumor mean ratio value of 1.6 ± 0.3, comparable with those previously reported for the same model [17] and [25].

Another important feature of solid tumor and in particular high-grade gliomas is represented by the presence of necrotic regions and hypoxic areas known to contribute to lesion progression and treatment resistance particularly to radiotherapy [26] and [27]. Indeed, the extension of hypoxic fraction is a negative prognostic factor for GBM patients [4]. According to the human pathology, F98 glioma presents central areas of necrosis surrounded by cluster of hypoxic regions and peritumoral edema [28]. In our study we demonstrated the presence of necrosis and hypoxia using post-mortem H&E staining and in vivo PET imaging respectively. The presence of hypoxic areas has been previously demonstrated using [^{18}F]MISO and [^{64}Cu]diacetyl-bis(N4-methylthiosemicarbazone) ([^{64}Cu]ATSM) in the rat C6 glioma model [29] and [30] but never in animals inoculated with F98 cells. In C6 rat model, Valable and colleagues reported [^{18}F]MISO tumor-to-non tumor ratio (T/NT) of 2.5 for lesion of 66 ± 30 mm^3[29] while in another study, based on the use of [^{64}Cu]ATSM, T/NT value was 3.8 for a median tumor volume of 192 mm^3[30]. For the first time we measured in vivo tumor hypoxic regions using PET in the F98 rat glioma model. Using [^{18}F]FAZA as radioligand, we observed at tumor onset a mean hypoxic volume of 38 ± 13 mm^3 with a mean T/B value of 2.2 ± 0.4. These parameters increased during time as indicated by the two animals that survived, performing a second PET study. The majority of clinical studies in patients were performed using [^{18}F]MISO as radioligand [4] and [31]. In these studies, the amount of tracer uptake positively correlated with tumor grade and negatively with the clinical outcome. The only study performed with [^{18}F]FAZA on patients with GBM reported T/B ratio values ranging from 1.9 to 15.6 [6].

In order to evaluate the relative distribution of hypermetabolic and hypoxic portion of tumor, we measured and compared [^{18}F]FDG and [^{18}F]FAZA distribution volume during illness progression.

Considering [^{18}F]FDG/[^{18}F]FAZA relationship, we observed that the distribution of the two radioligands only partially overlapped, being localized more in periphery the first and centrally the

last, particularly in the two animals were late PET study was performed. At tumor onset, [^{18}F]FAZA positive areas were localized in the core of the lesion and [^{18}F]FDG positive areas in adjacent more peripheral regions, inside the rim of T1-weighted MR images. During disease progression, [^{18}F]FAZA areas increased in a radial direction from the origin while [^{18}F]FDG positive areas moved toward the poles, following the tumor growth. Interestingly, a concomitant decrease of [^{18}F]FDG uptake was observed in the central part of the tumor, where the majority of [^{18}F]FAZA dependent signal was localized.

Like previously described in patients, areas of [^{18}F]FDG uptake were smaller than those detectable at T1-weighted MR imaging [13].

Regarding the relative distribution of hyper-metabolic and hypoxic areas in patients, in vivo reports on GBM are only in partial agreement [32] and [33]. Swanson et al. showed that [^{18}F]MISO positive areas were localized in peripheral regions outside the Gd-enhanced MRI regions, thus suggesting a role of hypoxia in driving tumor invasion [32], while Kawai et al. found [^{18}F]MISO positive areas in the centre of the lesion, inside Gd-enhanced areas [33]. In addition, in agreement with our results, a lack of correspondence between regional hypoxia and glucose metabolism has been demonstrated in patients with brain sarcoma or glioma [34]. Taken together, these data suggest that hypermetabolic cells represent the margin of tumor that progressively grows leaving a hypometabolic, but vital and hypoxic highly aggressive central core, despite the presence of clusters of necrosis. This information, even if doesn't allow a precise definition of tumor burden, which can be obtained using tracers as [^{11}C]Methionine or [^{18}F]FET, may be useful to identify the regional metabolic phenotype of lesion and the modification induced by treatment.

To further validate F98 model and to better understand [^{18}F]FAZA signals, we performed post-mortem analysis targeting two major players involved in tumor hypoxia: HIF-1α and VEGF. HIF-1α is a strong inducer of VEGF and the main regulator of cellular response to hypoxia. HIF-1α staining was highly expressed in peritumoral cells (mainly neurons) and in few cells in perinecrotic areas that, in F98 glioma, were located in the central core of tumor mass, as seen by imaging studies with MRI and H&E staining. Zagzag D. et al. [35] investigated the expression of HIF-1α in human glioma cell lines and tumor tissues, and observed the same distribution of this marker within the lesion. These results are also comparable to those obtained in clinical studies in which HIF-1α was detected in tumor cells that were near the areas of necrosis in GBM specimens [36]. We observed that all glioma cells showed positive staining for VEGF with cytoplasmatic distribution. Furthermore, also neurons located in cerebral parenchyma near oedematous areas were positive for VEGF, probably in response to hypoxic conditions of the tissue (as confirmed by MRI and [^{18}F]FAZA analysis). Results were reproducible in all implanted animals and were in agreement with clinical data [4], [31] and [33] in which VEGF expression was lower in normal compared to tumoral tissues. In these works, vascular proliferation in gliomas directly correlates with tumor grade and progression and inversely with overall survival, providing a possible use of VEGF as prognostic indicator.

We also decided to evaluate the expression of nestin, an intermediate filament (IF) protein, transiently expressed in neural stem/progenitor cells during the development of central nervous system. It has been shown that up-regulation of nestin is related to malignancy of several cancers, especially glioblastoma and it may be important for glial tumorigenesis for several mechanisms. Moreover the re-expression in tumor tissue greatly contributes to glioblastoma carcinogenesis and strictly correlates with high grade of malignancy in GBM [37] and [38]. In the same way, also our samples showed a strong nestin staining of all tumoral cells. In particular we showed that in small size tumors (early stage of the disease) there was a strong nestin component of tumoral cells. These data are in agreement with human GBM characteristics in which the strong tumoral nestin positivity is already present in early stages of tumor progression [39]. Furthermore, we studied the co-expression of nestin and GFAP. In normal brain, nestin is only expressed in early stages of neural progenitor maturation while, moving on toward differentiation mature glial (GFAP) or neural (neurofilament) markers are present. In tumors the expression of nestin and/or GFAP defines the grade of differentiation: nestin positive

means undifferentiated; nestin positive and GFAP positive mean intermediate state and GFAP positive differentiated. In our model, we found nestin and GFAP positive astrocytes surrounding the tumor, suggesting a response of stromal staminal cells to brain injury created by cancer mass (increase of astrogliosis) while in tumor cells a strong nestin expression (but not GFAP) was observed. Since the grade of differentiation inversely correlates with tumor malignancy, we can conclude that our model is really aggressive, as previously demonstrated by imaging and survival data.

Furthermore, to analyze the growth rate of the tumor we calculated the Ki-67 proliferative index which is now widely used as surrogate biomarker in clinical pathology and neuropathology diagnostic for several type of cancers to describe the number of cells that are actively growing [40]. A low proliferative index indicates a slower growth rate, thus suggesting a favourable prognosis. Our F98 model showed a Ki-67 index of 46%, confirming its high grade of aggressiveness and its good ability to reproduce histopathological findings of human glioblastomas.

In conclusion, F98 syngeneic rat model proved to be highly reproducible and a suitable preclinical model for primary glioblastoma as confirmed by both imaging and histological studies. Histopathological aspects of F98 model were comparable with those of human GBM and validated by MRI and PET imaging. Concerning diagnostic aspects, [^{18}F]FDG correlated with Ki-67 proliferative index: highly metabolic activity of glioma was strictly linked with high cellular division rate. Moreover, histological characteristics of hypoxia and vascularity (such as immunohistochemistry study with HIF-1α and VEGF) of tumor fitted with PET-[^{18}F]FAZA analysis showing that the major degree of hypoxia was located in correspondence of necrotic and oedematous areas.

Taken together, our results also suggest that in clinical practice different tumor biochemical information derived from PET (i.e. hypoxia and glucose consumption) should be associated to MRI in both pre-surgical and post-surgical stages to respectively guide lesion resection and monitor therapy outcomes ([^{18}F]FAZA for radionecrosis evaluation and [^{18}F]FDG for tumor recurrence). Co-registration of MRI and PET images and "Segmentation analysis" can be very helpful to refine tumoral areas and to monitor changes in metabolic/hypoxic characteristics of tumor during disease progression, confirming the specificity of PET technique and its usefulness in protocol setting of image-guided radiotherapy.

Acknowledgments

We thank Pasquale Simonelli for technical assistance with animal preparation and imaging experiments, Nadia El Assawy for animal euthanizing by perfusion, Dr. Maria Grazia Minotti and Dr. Mario Matarrese for radiochemical production and quality controls, Iadanza Antonella for MR images acquisition and elaboration, Dr. Loredana Serpe for pharmacological study in the animal model.

Supported by grants from: Regional AIRC project no. 6278; Italian University Ministry (FIRB RBIP06M8ZA_001); PIO (Programma Integrato Oncologia) project no. RFPS-2006-2-342023.8; NanoIGT Project (Converging Technologies 2007-Regione Piemonte). This study was part of the Eurobioimaging PCS.

Conflict of Interest

The authors declare that they have no conflict of interest.

References

[1] Central Brain Tumor Registry of the United States (CBTRUS) statistical report: primary brain and central nervous system tumors diagnosed in the United States in 2004–2008 (revised March 23, 2012. Available at: http://www.cbtrus.org/2012-NPCR-SEER/CBTRUS_Report_2004-2008_3-23-2012.pdf; 2012.

[2] Maher EA, Furnari FB, Bachoo RM, Rowitch DH, Louis DN, Cavenee WK, et al. Malignant glioma: genetics and biology of a grave matter. *Genes Dev* 2001; 15: 1311–33.

[3] Stewart LA. Chemotherapy in adult high-grade glioma: a systematic review and meta-analysis of individual patient data from 12 randomised trials. *Lancet* 2002; 359: 1011–8.

[4] Spence AM, Muzi M, Swanson KR, O'Sullivan F, Rockhill JK, Rajendran JG, et al. Regional hypoxia in glioblastoma multiforme quantified with [18F]fluoromisonidazole positron emission tomography before radiotherapy: correlation with time to progression and survival. *Clin Cancer Res* 2008; 14: 2623–30.

[5] Piert M, Machulla HJ, Picchio M, Reischl G, Ziegler S, Kumar P, et al. Hypoxiaspecific tumor imaging with 18F-fluoroazomycin arabinoside. *J Nucl Med* 2005; 46: 106–13.

[6] Postema EJ, McEwan AJ, Riauka TA, Kumar P, Richmond DA, Abrams DN, et al. Initial results of hypoxia imaging using 1-alpha-D: -(5-deoxy-5-[18F]-fluoroarabinofuranosyl)-2-nitroimida-zole (18F-FAZA). *Eur J Nucl Med Mol Imaging* 2009; 36: 1565–73.

[7] Semenza GL. Regulation of oxygen homeostasis by hypoxia-inducible factor 1. *Physiology (Bethesda)* 2009; 24: 97–106.

[8] Vaupel P, Harrison L. Tumor hypoxia: causative factors, compensatory mechanisms, and cellular response. *Oncologist* 2004; 9 (Suppl 5): 4–9.

[9] Wolf A, Agnihotri S, Micallef J, Mukherjee J, Sabha N, Cairns R, et al. Hexokinase 2 is a key mediator of aerobic glycolysis and promotes tumor growth in human glioblastoma multiforme. *J Exp Med* 2011; 208: 313–26.

[10] Flynn JR, Wang L, Gillespie DL, Stoddard GJ, Reid JK, Owens J, et al. Hypoxiaregulated protein expression, patient characteristics, and preoperative imaging as predictors of survival in adults with glioblastoma multiforme. *Cancer* 2008; 113: 1032–42.

[11] Patronas NJ, Di Chiro G, Kufta C, Bairamian D, Kornblith PL, Simon R, et al. Prediction of survival in glioma patients by means of positron emission tomography. *J Neurosurg* 1985; 62: 816–22.

[12] Barker 2nd FG, Chang SM, Valk PE, Pounds TR, Prados MD. 18-Fluorodeoxyglucose uptake and survival of patients with suspected recurrent malignant glioma. *Cancer* 1997; 79: 115–26.

[13] Tralins KS, Douglas JG, Stelzer KJ, Mankoff DA, Silbergeld DL, Rostomily RC, et al. Volumetric analysis of 18F-FDG PET in glioblastoma multiforme: prognostic information and possible role in definition of target volumes in radiation dose escalations. *J Nucl Med* 2002; 43: 1667–73.

[14] Soritau O, Tomuleasa C, Aldea M, Petrushev B, Susman S, Gheban D, et al. Metformin plus temozolomide-based chemotherapy as adjuvant treatment for WHO grade III and IV malignant glioma. *J BUON* 2011; 16: 282–9.

[15] Wick W, Weller M, Weiler M, Batchelor T, Yung AW, and Platten M. Pathway inhibition: emerging molecular targets for treating glioblastoma. *Neuro Oncol* 2011; 13: 566–79.

[16] Sibenaller ZA, Etame AB, Ali MM, Barua M, Braun TA, Casavant TL, et al. Genetic characterization of commonly used glioma cell lines in the rat animal model system. *Neurosurg Focus* 2005; 19: E1.

[17] Mathieu D, Lecomte R, Tsanaclis AM, Larouche A, Fortin D. Standardization and detailed characterization of the syngeneic Fischer/F98 glioma model. *Can J Neurol Sci* 2007; 34: 296–306.

[18] Reischl G, Ehrlichmann W, Bieg C, Solbach C, Kumar P, Wiebe LI, et al. Preparation of the hypoxia imaging PET tracer [18F]FAZA: reaction parameters and automation. *Appl Radiat Isot* 2005; 62: 897–901.

[19] Motta A, Damiani C, Del Guerra A, Di Domenico G, Zavattini G. Use of a fast EM algorithm for 3D image reconstruction with the YAP-PET tomograph. *Comput Med Imaging Graph* 2002; 26: 293–302.

[20] Boellaard R, Krak NC, Hoekstra OS, Lammertsma AA. Effects of noise, image resolution, and ROI definition on the accuracy of standard uptake values: a simulation study. *J Nucl Med* 2004; 45: 1519–27.

[21] Blanchard J, Mathieu D, Patenaude Y, Fortin D. MR-pathological comparison in F98-Fischer glioma model using a human gantry. *Can J Neurol Sci* 2006; 33: 86–91.

[22] Pardo FS, Aronen HJ, Fitzek M, Kennedy DN, Efird J, Rosen BR, et al. Correlation of FDG-PET interpretation with survival in a cohort of glioma patients. *Anticancer Res* 2004; 24: 2359–65.

[23] la Fougere C, Suchorska B, Bartenstein P, Kreth FW, and Tonn JC. Molecular imaging of gliomas with PET: opportunities and limitations. *Neuro Oncol* 2011; 13: 806–19.

[24] Tsuchida T, Takeuchi H, Okazawa H, Tsujikawa T, Fujibayashi Y. Grading of brain glioma with 1-11C-acetate PET: comparison with 18F-FDG PET. *Nucl Med Biol* 2008; 35: 171–6.

[25] Wang HE, Wu SY, Chang CW, Liu RS, Hwang LC, Lee TW, et al. Evaluation of F-18-labeled amino acid derivatives and [18F]FDG as PET probes in a brain tumorbearing animal model. *Nucl Med Biol* 2005; 32: 367–75.

[26] Jensen RL. Brain tumor hypoxia: tumorigenesis, angiogenesis, imaging, pseudoprogression, and as a therapeutic target. *J Neurooncol* 2009; 92: 317–35.

[27] Stupp R, Mason WP, van den Bent MJ, Weller M, Fisher B, Taphoorn MJ, et al. Radiotherapy plus concomitant and adjuvant temozolomide for glioblastoma. *N Engl J Med* 2005; 352: 987–96.

[28] Wen PY, Kesari S. Malignant gliomas in adults. *N Engl J Med* 2008; 359: 492–507.

[29] Valable S, Petit E, Roussel S, Marteau L, Toutain J, Divoux D, et al. Complementary information from magnetic resonance imaging and (18)F-fluoromisonidazole positron emission tomography in the assessment of the response to an antiangiogenic treatment in a rat brain tumor model. *Nucl Med Biol* 2011; 38: 781–93.

[30] Sheehan JP, Popp B, Monteith S, Toulmin S, Tomlinson J, Martin J, et al. Trans sodium crocetinate: functional neuroimaging studies in a hypoxic brain tumor. *J Neurosurg* 2011; 115: 749–53.

[31] Cher LM, Murone C, Lawrentschuk N, Ramdave S, Papenfuss A, Hannah A, et al. Correlation of hypoxic cell fraction and angiogenesis with glucose metabolic rate in gliomas using 18F-fluoromisonidazole, 18F-FDG PET, and immunohistochemical studies. *J Nucl Med* 2006; 47: 410–8.

[32] Swanson KR, Chakraborty G, Wang CH, Rockne R, Harpold HL, Muzi M, et al. Complementary but distinct roles for MRI and 18F-fluoromisonidazole PET in the assessment of human glioblastomas. *J Nucl Med* 2009; 50: 36–44.

[33] Kawai N, Maeda Y, Kudomi N, Miyake K, Okada M, Yamamoto Y, et al. Correlation of biological aggressiveness assessed by 11C-methionine PET and hypoxic burden assessed by 18F-fluoromisonidazole PET in newly diagnosed glioblastoma. *Eur J Nucl Med Mol Imaging* 2011; 38: 441–50.

[34] Rajendran JG, Mankoff DA, O'Sullivan F, Peterson LM, Schwartz DL, Conrad EU, et al. Hypoxia and glucose metabolism in malignant tumors: evaluation by [18F]fluoromisonidazole and [18F]fluorodeoxyglucose positron emission tomography imaging. *Clin Cancer Res* 2004; 10: 2245–52.

[35] Zagzag D, Zhong H, Scalzitti JM, Laughner E, Simons JW, Semenza GL. Expression of hypoxia-inducible factor 1alpha in brain tumors: association with angiogenesis, invasion, and progression. *Cancer* 2000; 88: 2606–18.

[36] Chan AS, Leung SY, Wong MP, Yuen ST, Cheung N, Fan YW, et al. Expression of vascular endothelial growth factor and its receptors in the anaplastic progression of astrocytoma, oligodendroglioma, and ependymoma. *Am J Surg Pathol* 1998; 22: 816–26.

[37] Strojnik T, Rosland GV, Sakariassen PO, Kavalar R, Lah T. Neural stem cell markers, nestin andmusashi proteins, inthe progression of human glioma: correlation of nestin with prognosis of patient survival. *Surg Neurol* 2007; 68: 133–43 discussion 43–4.

[38] Yang XH, Wu QL, Yu XB, Xu CX, Ma BF, Zhang XM, et al. Nestin expression in different tumours and its relevance to malignant grade. *J Clin Pathol* 2008; 61: 467–73.

[39] Jang T, Sathy B, Hsu YH, Merchant M, Recht B, Chang C, et al. A distinct phenotypic change in gliomas at the time of magnetic resonance imaging detection. *J Neurosurg* 2008; 108: 782–90.

[40] Haapasalo J, Mennander A, Helen P, Haapasalo H, Isola J. Ultrarapid Ki-67 immunostaining in frozen section interpretation of gliomas. *J Clin Pathol* 2005; 58: 263–8.